Applied Catalysis B: Environmental 252 (2019) 152–163

Contents lists available at ScienceDirect

Applied Catalysis B: Environmental

journal homepage: www.elsevier.com/locate/apcatb

Synthesis of visible light responsive iodine-doped mesoporous TiO_2 by using biological renewable lignin as template for degradation of toxic organic pollutants

Xiaoyun Chen[a], Huizhi Sun[a], Jubin Zhang[a], Osman Ahmed Zelekew[b,*], Dongfang Lu[a], Dong-Hau Kuo[c,*], Jinguo Lin[a,*]

[a] College of Materials Engineering, Fujian Agriculture & Forestry University, Fuzhou, 350002, China
[b] Department of Materials Science and Engineering, Adama Science and Technology University, Adama, Ethiopia
[c] Department of Materials Science and Engineering, National Taiwan University of Science and Technology, No.43, Sec. 4, Keelung Road, Taipei, 10607, Taiwan

ARTICLE INFO

Keywords:
I-Doped
Lignin template
Mesoporous
TiO_2
Visible light

ABSTRACT

The visible light responsive I-doped mesoporous TiO_2 (I/TiO_2-T) catalysts were synthesized by facile hydrolysis method with lignin as a template. The resulting I/TiO_2-T catalysts synthesized from different amounts of I as a dopant and lignin as a template were characterized by X-ray photoelectron spectroscopy (XPS), X-ray diffraction (XRD), transmission electron microscopy (TEM), UV–vis diffuse spectroscopy (DRS), Fourier transform infrared spectroscopy (FTIR), photoluminescence (PL), and electrochemical impedance spectroscopy (EIS). The photocatalytic activities of the resulting catalysts were investigated by the degradation of p-chlorophenol under artificial visible light irradiation. The results showed that the lignin-templated TiO_2 with a suitable amount of I-doping (I/TiO_2-T) had higher catalytic activity than the catalyst prepared form I-doped TiO_2 without lignin template (I/TiO_2). Complete degradation of p-chlorophenol was achieved by I/TiO_2-T with suitable amount of I-doping at 60 min. However, 95.7, 10.7, and 5.5% of the p-chlorophenol was degraded with I/TiO_2, TiO_2-T, and P25 catalysts, respectively, under 140 min visible light irradiation. The enhanced catalytic activities of the samples with template and I-doping may be due to the small grain size and high specific surface area of the catalysts. The band gap and the electrical properties of TiO_2 also could be adjusted with I-doping. The I-doped TiO_2 with the extrinsic I^{5+}-to-Ti^{4+} and the iodine-to-oxygen donor defects could be excited by visible irradiation for efficient pollutants degradation. A possible photocatalytic mechanism for the degradation of the pollutants with I/TiO_2-T under visible light irradiation was also proposed.

1. Introduction

Nowadays, photocatalysis has been considered as an alternative method for the decontamination of wastewater and confirmed to be a technically feasible cleanup process [1,2]. Mainly, semiconductor based photocatalysts have been used extensively in the photocatalysis technologies [3–6]. Among semiconductor photocatalysts, titanium dioxide (TiO_2) has been widely studied due to its photocatalytic activity, low toxicity, high chemical stability, and low cost [7–10]. It is known that TiO_2 is stable and highly active under ultraviolet (UV) light. However, the UV solar light incident on the earth's surface is only about 5% [11]. The wider band gap energy and lower solar energy conversion efficiency of TiO_2 also greatly limits the utilization of visible light solar energy for practical applications [12–15]. Hence, the synthesis of TiO_2 photocatalysts with good visible light response, large specific surface area, and high quantum efficiency is the major concern for the scientific community [16–18].

The design of heterogeneous photocatalyst for effective utilization of visible light in the wastewater treatment technology becomes the main research area, recently [19]. For this reason, researchers tried to improve the light absorption range for TiO_2 semiconductor with different methods [20–22]. Among the methods used, the p-n nanoheterojunction formation, doping, and making composite with lower band gap semiconductor materials were reported [20–23]. There are also many reports on the improvement of the visible light response of TiO_2 with iodine doping [24–26]. Liu et al. [27] reported the iodine-doped titania with bicrytalline framework for effective utilization of visible light. Su et al. [28] also prepared the multivalency iodine doped TiO_2

* Corresponding authors.
E-mail addresses: osman.ahmed@astu.edu.et (O. Ahmed Zelekew), dhkuo@mail.ntust.edu.tw (D.-H. Kuo), fjlinjg@126.com (J. Lin).

https://doi.org/10.1016/j.apcatb.2019.04.034
Received 18 March 2019; Accepted 12 April 2019
Available online 13 April 2019
0926-3373/

via a combination of deposition–precipitation and hydrothermal treatment process. Usseglio et al. [29] also synthesized the nanovoid-structured of TiO_2 with addition of iodine, which could absorb the visible light spectrum. The iodine doped anatase TiO_2 photocatalyst with visible light response was also prepared by Liu et al. [30]. However, I-doping on TiO_2 only may not be sufficient and effective for catalytic activities. Hence, it is important to design porous and active catalyst which could have the ability to absorb visible light source efficiently.

The researchers also tried to combine TiO_2 with biological renewable resource, which could make the material more porous. For this reason, the biological renewable resources such as cellulose and lignin as template were used to improve the porosity of TiO_2 [31–33]. Cai et al. [34] used cellulose nanofibrils-based aerogel template for the synthesis of highly porous titanium dioxide. Zhou et al. [35] also used nanocrystal cellulose as a morphology inducer for the synthesis of square nano-TiO_2. The mesoporous TiO_2 films were also prepared from titanium tetrabutyloxide and cellulose by Miao et al. [36]. The synthesis of N and N—F co-doped mesoporous TiO_2 photocatalysts by using nanocellulose as template were also reported [37]. Recently, our group also reported on the biological renewable resource of un-modified lignin which obtained from the paper-making industry black liquid as template for the preparation of mesoporous TiO_2 and used for the degradation of phenol [38]. However, the reports on using lignin as a template were very few and there were no reports on the synthesis of non-metallic doped TiO_2 with lignin as template for visible light-responsive catalyst.

In this work, we report the synthesis of mesoporous iodine-doped TiO_2 by using lignin as a template which is separated from the black liquor of paper-making industries. The resulting catalysts were characterized by different instruments. The photocatalytic activities of the I/TiO_2-T were also examined by the degradation of p-chlorophenol, nitrobenzene, and phenol under visible light and solar light irradiation. Moreover, a possible mechanism for the enhanced performance of the I/TiO_2-T was also proposed.

2. Experimental methods

2.1. Chemicals

All chemicals and reagents in this experiments were analytical grade and used without further purifications.

2.2. Lignin template preparation

The preparation of lignin template was from the black liquor of paper-making industries of Fujian Qingzhou mills, China, according the method reported by Chen et al. [38]

2.3. Catalysts preparation

In a typical synthetic procedure, 10 ml of $TiCl_4$ was slowly dropped into a beaker containing 200 mL (2.5 g/L) of lignin aqueous solution and stirred for 30 min. Then, the mixture was heated at 80 °C for another 30 min with continuous stirring and the pH of the mixture was then adjusted to pH = 7 with addition of ammonium hydroxide. After stirring for another 30 min, the resulting precipitate was washed with distilled water. Subsequently, the mixture will be used for the preparation of I-doped TiO_2 lignin templated composite.

The resulting lignin and $TiCl_4$ mixture synthesized above was mixed with KIO_3 and ethanol, and stirred for 2 h. The solution was kept at room temperature for 10 h. Different composition with the n(Ti)/n(I) molar ratios were prepared and the ratios were 5/1, 5/2, and 5/3. The resulting products were dried under vacuum at 85 °C, and calcined at 500, 600, 700, 800, and 900 °C in air for 2 h. The Yellow-colored I-doped TiO_2 with lignin as template was obtained and labeled as I/TiO_2-T. For comparison, I-doped TiO_2 catalyst without lignin template was also prepared under the same procedure and labeled as I/TiO_2. Moreover, the lignin-templated TiO_2 without iodine doping was also prepared with similar procedure and condition and labeled as TiO_2-T.

2.4. Characterization of catalysts

The crystal structures of the prepared catalysts were characterized by Rigaku X-ray diffractometer with the Cu $K\alpha$ radiation (λ = 1.5406 Å) sources. The morphologies and microstructure of the samples were examined by Transmission electron microscopy (TEM, Tecnai G2 F20). The XPS analysis was performed by the Physical Electronics PHI5700 photoelectron spectrometer under the Al $K\alpha$ X-rays ($h\nu$ = 1486.6 eV) radiation and calibrated with carbon. The UV–vis DRS analysis was conducted by TU-1901 UV–vis spectrophotometer equipped with an integrating sphere. The Fourier transform infrared (FTIR) spectra collection was conducted by Nicolet-380 spectrometer with embedding in KBr pellet. The nitrogen adsorption-desorption experiments were conducted by ASAP 2020 porosity and specific surface area analyzer after the sample degassed at 200 °C for 2 h. Specific surface area and pore size distribution were also calculated according to the BET and BJH formulas, respectively. The surface acidity of TiO_2-T and I/TiO_2-T were also determined by n-butylamine titration method by using methyl red as indicator according to the literature [39].

2.5. Electrochemical measurements

The electrochemical impedance measurements of the catalysts were performed by SP-300 Biologic Science with 0.1 mol/L KCl electrolyte solution and three electrodes system. The glassy carbon, Ag/AgCl/KCl, and platinum plate electrodes were used as the working, counter and reference electrodes, respectively. For the preparation of slurry, 5 mg of the catalyst was dispersed in 2 mL nafion solution by ultrasonication bath for 10 min. After dispersed, the solution was dropped on the surface of working electrode and dried in the oven at 85 °C for 10 min. The initial and the final frequencies of the system were adjusted to 100 mHz, and 200 kHz, respectively. The experiment was performed with the voltage amplitude at 10 mV, and the voltage range from −1 to 1 V.

2.6. Evaluation of produced hydroxyl radicals

The amount of hydroxyl radicals (·OH) determination was conducted according to the literature [30,40–42]. In a typical procedure, 50 mg of catalyst was dissolved in 50 mL of aqueous solution containing 2 mmol NaOH and 0.5 mmol terephthalic acid. The mixture was stirred and illuminated for 1 h with 350 W Xe lamp (λ shorter than 400 nm was filtered). Then, 10 mL of solution was centrifuged and used for fluorescence spectrum measurements. The fluorescence spectra of generated 2-hydroxyterephthalic acid were measured on a Varian Cary-Eclipse 500 fluorescence spectrophotometer. The working excitation light in the measurement of fluorescence spectra was 315 nm.

2.7. Photocatalytic activity measurements

The photocatalytic activity measurements were performed in an in-home made quartz jacketed reactor as reported according to Chen et al. [43]. The photocatalytic activities of the prepared catalysts were evaluated by the degradation of p-chlorophenol aqueous solution. In the typical procedure, 0.125 g catalyst was dispersed into 250 mL of p-chlorophenol (50 mg/L) solution in glass reactor. The mixture was then stirred for 30 min in dark condition to confirm the adsorption-desorption equilibrium between the pollutant and the catalyst. Then, xenon lamp (350 W) after filtered the wavelengths lower than 400 nm was used as sources of visible light. Air was bubbled into the reactor during reaction in order to mix solution with dissolve oxygen. Then, 5 ml

aliquot was taken in every 20 min and centrifuged at 4000 r/min for 5 min for kinetic studies. The catalytic performance of the catalyst was also tested for nitrobenzene, and phenol pollutants and the procedure were similar with that of p-chlorophenol used above. The supernatant concentrations of p-chlorophenol, nitrobenzene, and phenol were examined by using a Primaide high performance liquid chromatography with a Kromasil C_{18} (250 mm × 4.6 mm, 5 μm) column. The mobile phase was methanol-water (80 : 20, v/v) mixture at a flow rate of 1 ml/min. 20 μl was set as an injection volume with a column temperature of 25 °C. The detection wavelengths for p-chlorophenol, nitrobenzene, and phenol were set at 280, 262, and 270 nm, respectively. Moreover, the pH of the aqueous solutions were also adjusted with 0.1 mol/L HNO_3 and NaOH and checked by PHS-3C pH meter.

Photocatalytic activity under solar light was also tested and 0.125 g catalyst was added into 250 ml 50 mg/L p-chlorophenol solution in a petri dish of 15 cm in diameter. The reactant mixture was stirred for 30 min to obtain the adsorption-desorption equilibrium between p-chlorophenol and catalyst. Then, the petri dish sealed with plastic wrap was exposed to the sunlight for testing from 9:00 AM till 3:00 PM in 8 August at Fujian, China. The temperature was 25–35 °C.

The reusability of I/TiO_2-T catalyst was also performed by adding 0.125 g catalyst into 250 mL p-chlorophenol (50 mg/L) solution. The reactant mixture was magnetically stirred in the dark for 30 min, and then reacted under visible light irradiation for 60 min. After filtering the solution, the remaining catalyst was reused for the next photocatalytic reaction. Moreover, the total organic carbon (TOC) content in the reaction samples was measured with a Shimadzu SSM-5000 A carbon analyzer.

3. Results and discussion

3.1. Phase structural and morphology analysis

The crystal structure and the phases of the catalysts were identified by XRD. Fig. 1 shows the XRD diffraction patterns of TiO_2, I-TiO_2, and I/TiO_2-T calcined at 600 °C. As it is observed from Fig. 1, the characteristic peak positions at 25.27° and 27.48° for anatase and rutile, respectively, were not affected by I-doping. The major rutile phase was clearly observed without I-doping and template in the prepared samples. However, the I-doped TiO_2 (I-TiO_2) had smaller rutile phases as

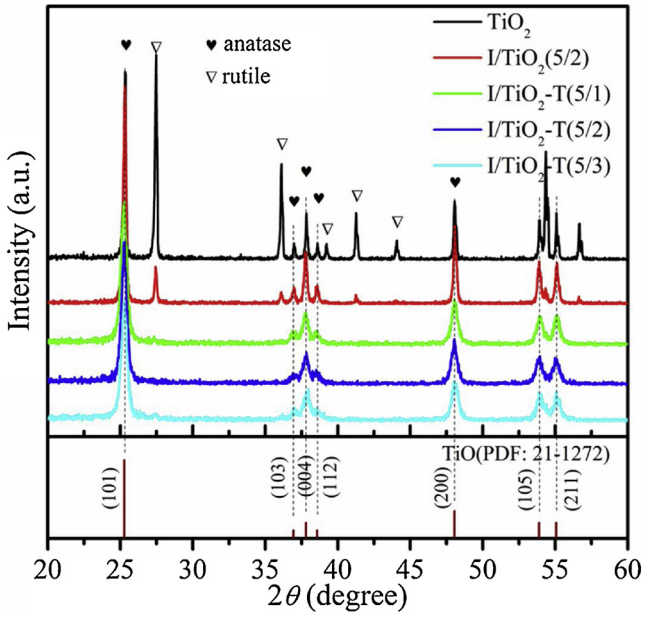

Fig. 1. XRD patterns of TiO_2, I/TiO_2, and I/TiO_2-T with different I-doping amounts calcined at 600 °C.

compared to TiO_2 without I-doped and template. Moreover, the I/TiO_2-T synthesized with I-doped and lignin as template had well crystallized anatase phase. The average crystal sizes of the catalysts were also calculated by Scherrer formula and showed in Table 3. As we have seen from Table 3, the crystalline size of the I/TiO_2-T was about 11 nm. However, the crystalline size of the template-free TiO_2, I-free TiO_2-T, and I/TiO_2 were 30.5, 16.7, and 17.5 nm, respectively. The results indicate that the I-doping and the lignin template can make the TiO_2 crystalline size smaller, and also inhibit the phase transformation from anatase to rutile phase. The inhibition of the phase transformation may be due to Ti-O-I bond formations, and also the doped I^{5+} ions form a ligand with $Ti(OH)_n$. This phenomena also retard the rutile phase formation and make the TiO_2 crystalline size smaller [44]. The results indicate that the TiO_2 anatase phase, similar with the reported standard (JCPDS No. 21-1272), is formed in the presence of both I-doping and lignin.

The morphologies of the catalyst were also shown in Fig. 2. As it is observed from Fig. 2a, the TEM image of I/TiO_2 catalyst synthesized without lignin as a template had a considerable degree of agglomeration and larger particles size (50~200 nm). However, the I/TiO_2-T catalyst synthesized in the presence of lignin as template showed superior particle size dispersion and had several smaller pores (Fig. 2b). These pores enable the rapid transfer of photogenerated carriers to the particle surface and participate in the photocatalytic reaction [45,46]. Fig. 2c also exhibits the HR-TEM image of I/TiO_2-T. The d-spacing value of 3.52 Å is matched with the standards of TiO_2 anatase phase (JCPDS No. 21-1272).

3.2. XPS analysis

In order to confirm the chemical composition of the catalysts, the XPS analysis was performed. The chemical states and compositions of the I/TiO_2-T (5 : 2) calcined at 600 °C were tested and the results are shown in Fig. 3. The XPS survey spectrum of the I/TiO_2-T (5 : 2) indicated the presence of Ti, I, C, and O elements in the prepared sample (Fig. 3a). Moreover, the I 3*d* high resolution XPS spectrum in the I/TiO_2-T catalyst was also observed (Fig. 3b). The peaks at 623.6 and 635.2 eV binding energies correspond to I $3d_{5/2}$ and I $3d_{3/2}$, respectively, and indicate the presence of I^{5+} in the composition. The weaker satellite peaks at 619.9 eV (I $3d_{5/2}$) and 631.5 eV (I $3d_{3/2}$) also confirm the presence of I^- in the sample [22,25,47,48]. The result is also matched with the literature and confirms the I^{5+}/I^- pairs formation for I-doped TiO_2. It is also illustrated that the I^{5+} ions substitute for Ti^{4+} and exists in the I–O–Ti bond [42,49]. This bonding structure can form a narrow band gap that enhances the visible light catalytic activity [50–52]. Moreover, Fig. 3c also shows the Ti 2*p* XPS spectrum of TiO_2-T and I/TiO_2-T(5/2) calcined at 600 °C. As it is observed, the binding energies of Ti^{4+} $2p_{3/2}$ and Ti^{4+} $2p_{1/2}$ of TiO_2-T were 458.7 and 464.5 eV, respectively. However, the binding energies of Ti^{4+} $2p_{3/2}$ and Ti^{4+} $2p_{1/2}$ of I/TiO_2-T(5/2) were 458.4 and 464.2 eV, respectively. The result indicates that I-doping makes the binding energies of Ti 2*p* lower. The decrease in the binding energy of Ti 2*p* may be due to the formation of new chemical bond of I–Ti–O. It is also known that the electro-negativity of I is smaller than that of O, hence, the electron density around Ti and the screening effect will decreases, which results in the decrease of binding energy of Ti 2*p* [53,54]. The smaller peaks shown in the lower side of Ti $2p_{3/2}$ (457.5 eV) and Ti $2p_{1/2}$ (463.1 eV), are also attributed to Ti^{3+}. The Ti^{3+} is formed to maintain the electro-neutrality of the system cause by I^{5+} substituting Ti^{4+} [55]. Fig. 3d also indicates the O 1*s* XPS spectra of I/TiO_2-T and TiO_2-T. The peaks located at 529.6 eV and 531.1 eV are attributed to the lattice oxygen and hydroxyl oxygen, respectively. In order to verify whether carbon remained in the catalyst, we analyzed the XPS C 1*s*. Fig. 3e shows the C 1*s* high resolution XPS spectra of the I/TiO_2 catalyst without lignin template and I/TiO_2-T with lignin template. It was obvious that the peaks at 284.6 eV for I/TiO_2 and I/TiO_2-T were similar, the position and shape of the

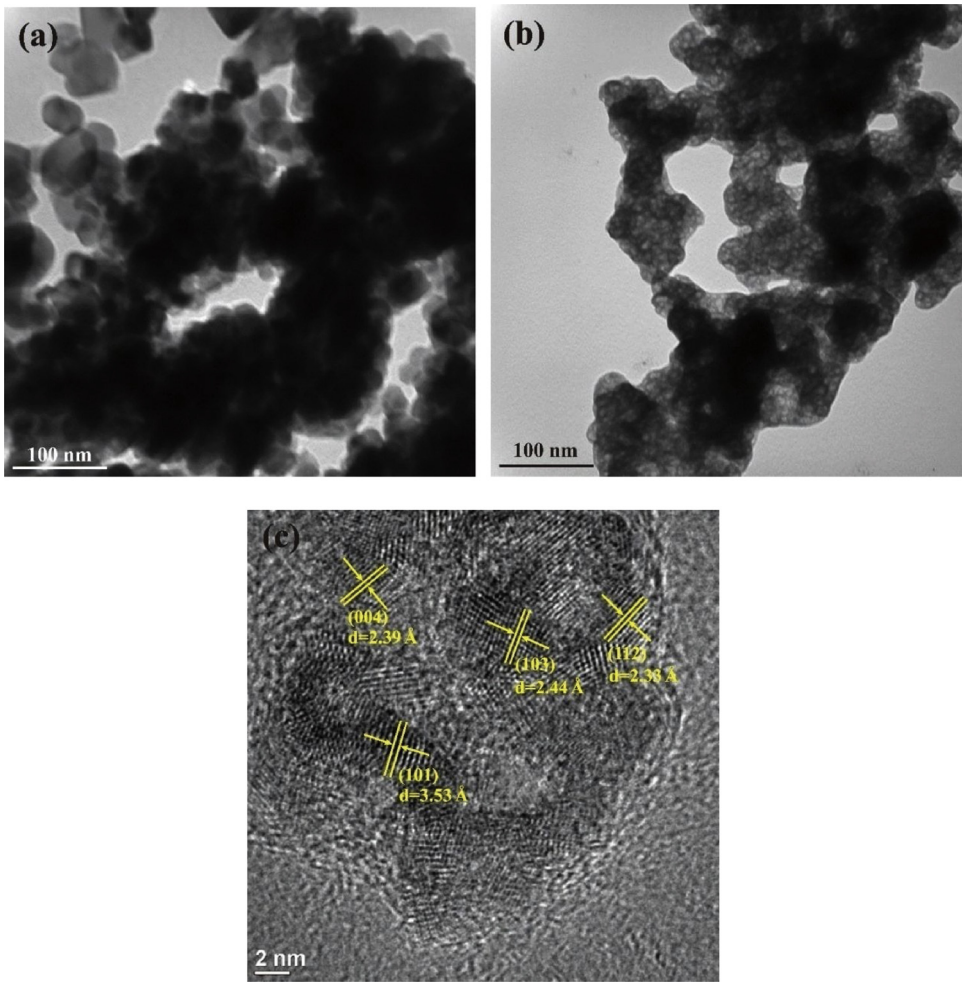

Fig. 2. TEM image of (a) I/TiO_2, (b) I/TiO_2-T and (c) HR-TEM image of I/TiO_2-T catalysts.

peaks had no significant changes, and also no extra peaks were observed, which confirmed that the lignin was all burned out without any C left in catalyst.

The ratios of lattice oxygen and hydroxyl oxygen in the sample were also calculated according to the peak area and listed in Table 1. As we have seen from Table 1, the amount of surface hydroxyl group increases but the lattice oxygen decreases in TiO_2 during I-doping. The surface hydroxyl group of TiO_2 is the photogenerated holes scavenger. Furthermore, the TiO_2 can generate more reactive ·OH radical and enhances the efficiency of photocatalytic oxidation [56]. The amount of Ti decreases with the increasing the amount of iodine doping. However, the amount of lattice oxygen in I/TiO_2-T was significantly reduced as we increased the amount of I-doping.

The acidity measurements of the catalyst surface are also shown in Table 2. As it is observed from the table, the surface acidity of TiO_2 is greatly improved with I doping. This result further confirms the XPS analysis in which the surface hydroxyl group of TiO_2 increased with the I doping. It was reported that the there was a relationship between the photocatalytic activity and the number and strength of acid sites [57].

3.3. FTIR analysis

Fig. 4 shows the FTIR spectra of TiO_2-T and I/TiO_2-T with different amounts of I-doping calcined at 600 °C. The FTIR peaks positioned at 3422 and 1631 cm^{-1} corresponds to the hydroxyl stretching and bending vibration of water or hydroxyl group absorbed on the surface of the catalyst. It is also indicated that the I-doping causes the hydroxyl stretching and bending vibration of absorption peaks stronger and the peaks also enhanced with increasing the amount of I-doping. The results also further confirms the XPS and surface acidity analysis in which the number of hydroxyl groups on the surface of TiO_2 increased after I-doping. Moreover, the strong absorption was also observed in range of 480˜- 680 cm^{-1} and this absorption peak may be due to the lattice stretching vibrations of anatase O-Ti-O bonding in TiO_2. The broader peaks located at 3151, 1401 cm^{-1} also correspond to H—I—H stretching and bending vibration from water or surface hydroxyl groups absorbed on the surface of the catalyst [49,58]. A new characteristic absorption peak at 1047 cm^{-1} was also observed, and the intensity of the adsorption peak increased with the increasing of the amount of I-doping [49]. Liu et al. [59] and Chen et al. [37] reported the FTIR characteristic absorption peak of Ti-O-N bond of N-doped TiO_2 catalyst appears at 1059 cm^{-1}. Chen et al. [43,60] reported the FTIR characteristic absorption peak of Ti-O-S bond of S-doped TiO_2 catalyst appears at 1031 cm^{-1}. The FTIR characteristic peak of Ti-O-C bond at the interface between TiO_2 and activated carbon appears at 1020 cm^{-1} [49,61]; Zhang et al. [62] and Chen et al. [51] reported the FTIR characteristic peak of Ti-O-Si bond of the TiO_2/SiO_2 composite catalyst appears at 949 cm^{-1}. We know that the electronegativity of I is about 2.66, which is higher than that of Si (1.90), C (2.55), S (2.58), and small than N (3.05). The Ti-O-I absorption peak position will be between the absorption peaks of Ti-O-C, Ti-O-Si, Ti-O-S, and the Ti-O-N bond. Hence, the absorption peak at 1047 cm^{-1} is corresponds to the Ti-O-I on the TiO_2 surface. The peak located at 3151, 1401 cm^{-1} corresponds to H—I—H stretching and bending vibration from water or surface hydroxyl groups absorbed on the surface of the catalyst [49,58].

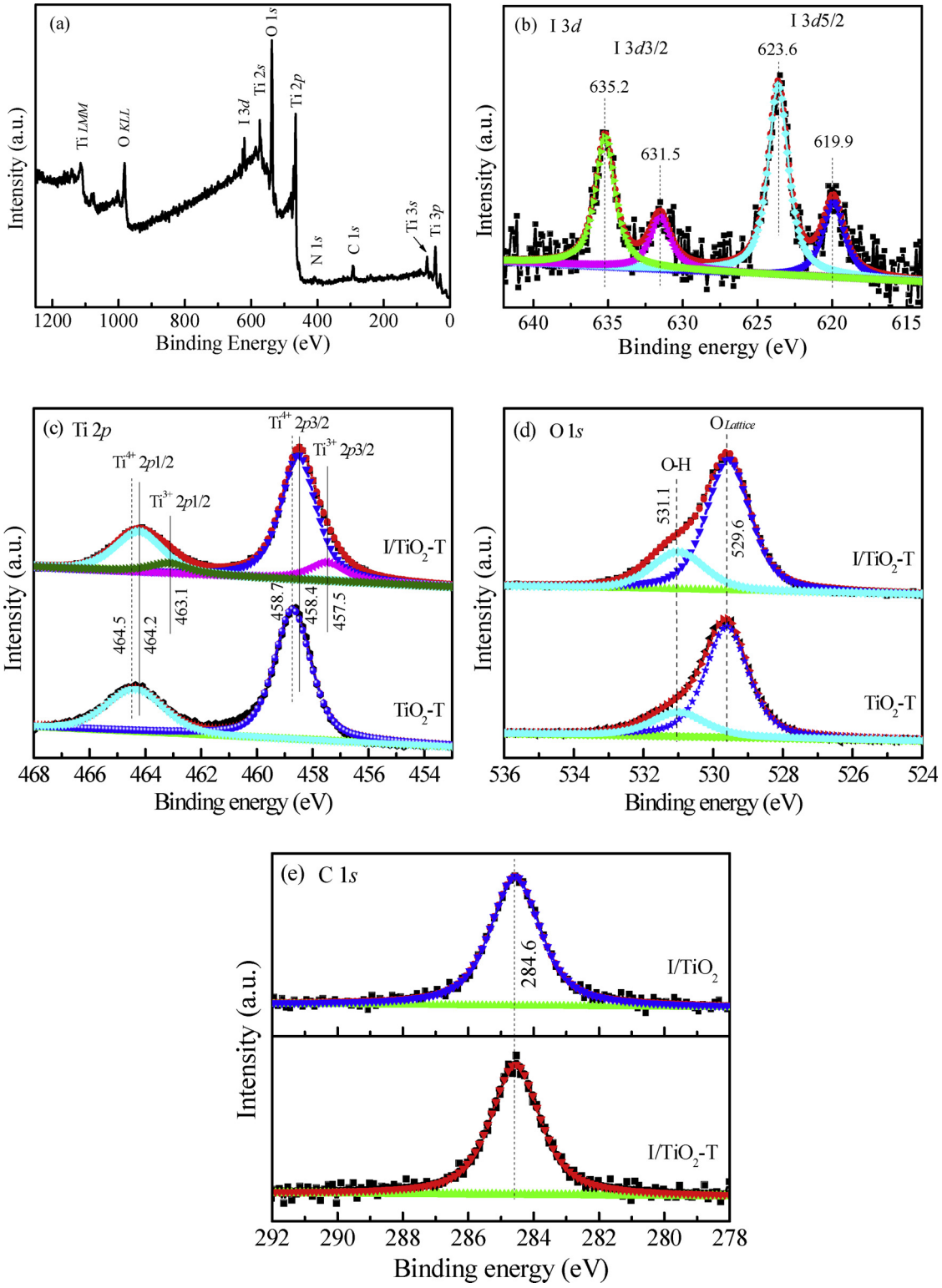

Fig. 3. (a) The survey XPS spectra of I/TiO_2-T and the high resolution XPS spectra of (b) I 3*d*, (c) Ti 2*p*, (d) O 1*s*, and (e) C 1*s*.

3.4. UV–vis and photoelectrochemical properties analysis

Fig. 5a, shows the UV–vis DRS of TiO_2-T and I/TiO_2-T with different amount of I-doping calcined at 600 °C. The TiO_2-T catalyst showed the absorption in the UV range. However, the I/TiO_2-T had the ability to absorb the visible light ranges. The absorption of the catalyst increased with increasing the amount of I-doping in the visible light range. The first derivatives of DRS spectra were used to obtain the inflection points of the catalysts and the E_g values were calculated according to the band gap formula of E_g (eV) = 1240/λ [62]. The first inflection point was 3.1 ~- 3.2 eV and the second one was 2.2 ~- 2.5 eV. The results were shown in Table 3.

In order to investigate the efficiency of the charge transfer between the interface of catalyst that coated on the working electrode and electrolyte solution, the electrochemical impedance was performed. Fig. 5b shows the EIS of I/TiO_2-T with different mounts of I-doping. The

Table 1
The elements analyses of catalysts.

Catalysts	Ti	O	I	O^{2-} (%)	OH^- (%)	$n(OH^-)/n(O^{2-})$ (%)
TiO_2	27.55	72.45	0.00	79.69	20.31	25.49
I-TiO_2(5/2)	26.62	72.47	0.91	73.64	26.36	35.80
I/TiO_2-T(5/1)	26.99	72.48	0.53	75.05	24.95	33.24
I/TiO_2-T(5/2)	26.34	72.46	1.20	73.92	26.08	35.28
I/TiO_2-T(5/3)	25.85	72.43	1.72	72.23	27.77	38.45

Randles fitting was also performed to estimate the electron transfer resistance for each catalyst. The symbols of Q2, R1, and R2 were related to the double layer capacitance, electrolyte resistance, and electron transfer resistance, respectively. Based on the Randles fitting, the calculated electron transfer resistance values of TiO_2-T, I/TiO_2-T(5/1), I/TiO_2-T(5/2), I/TiO_2-T(5/3) were 6.24 KΩ, 5.29 KΩ, 2.53 KΩ, and 3.91 KΩ, respectively. The lowest electron transfer resistance was found to be 2.53 KΩ for I/TiO_2-T(5/2). The EIS measurements indicated that the most efficient electron transfer in the interfaces between electrode and electrolyte was achieved for the I/TiO_2-T(5/2) catalyst. Hence, the I/TiO_2-T(5/2) catalyst is expected to have the highest catalytic activity for oxidation degradation reaction.

3.5. Hydroxyl radical analysis

In order to investigate the mechanism of the photocatalytic activity of the I/TiO_2-T catalyst, it is important to determine the amount of ·OH formed with photo-illuminated light. The resulting ·OH formed was detected by a photoluminescence (PL) method using terephthalic acid as a probe molecule. As we have seen from Fig. 6, the I/TiO_2-T catalysts with different amount of I-doping produced different amount of hydroxyl radicals under the same conditions. The order for the amount of ·OH produced with the catalysts were I/TiO_2-T(5/2) > I/TiO_2-T(5/3) > I/TiO_2-T(5/1) > I/TiO_2 (5/2) > TiO_2-T. This indicated that the optimum amount of I-doped used to enhance the visible light catalytic activity of TiO_2 and prevents the direct recombination of the photogenerated electrons and holes. Hence, the lower recombination rate of the photogenerated electrons and holes will enhance the photocatalytic activity of the catalyst [63].

3.6. BET surface area and pore volume analysis

Nitrogen adsorption–desorption isotherms and pore size distributions of the I/TiO_2, TiO_2-T, and I/TiO_2-T are shown in Fig. 7. The TiO_2-T and I/TiO_2-T catalysts showed the type IV isotherms, while the type V isotherms indicated for me /TiO_2; hence, the samples had mesoporous. Moreover, the H1-type hysteresis loop with the pressure range between 0.45 and 0.95 exhibits for the curve TiO_2-T and I/TiO_2-T and indicated that the pore type of TiO_2-T and I/TiO_2-T was cylinder-like [64]. However, the curve of I/TiO_2 exhibits between H3-type hysteresis loop at pressure range between 0.70 and 0.95 and it is indicates that the pore type of I/TiO_2 is wedge-like.

The BJH pore size distributions curve was also shown in Fig. 7b. The pore size distributions of TiO_2-T and I/TiO_2-T samples were narrower than that of pure I/TiO_2. The pore size distribution of the TiO_2-T and I/TiO_2-T catalysts was between 1 nm and 10 nm, while for the I/TiO_2 catalyst it was between 1 nm and 20 nm. The S_{BET} of TiO_2, I/TiO_2, TiO_2-T and I/TiO_2-T catalysts were about 23, 40, 122, and 149 m^2/g, respectively. Moreover, the pore volume of the TiO_2, I/TiO_2, TiO_2-T, and I/TiO_2-T were about 0.083, 0.131, 0.296, and 0.350 m^3/g, respectively. The results showed that the I-doped and lignin template increased the specific surface area and pore volume of I/TiO_2-T. However, the amount of doping iodine is little effect on the S_{BET} and pore volume. Table 3 shows the S_{BET} and the pore volumes of the TiO_2, I/TiO_2, TiO_2-T, and I/TiO_2-T samples.

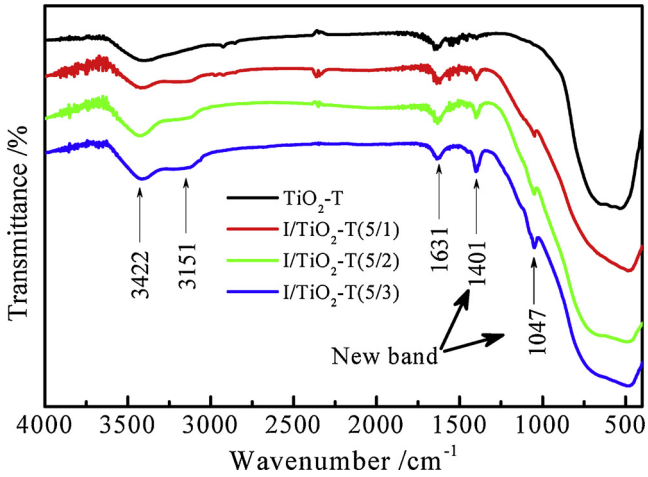

Fig. 4. FTIR spectra of TiO_2-T and I/TiO_2-T catalysts.

3.7. Photocatalytic activities

The photocatalytic activities of TiO_2 could be influenced by, porosity, band gap, surface area, crystal structure and the amount of hydroxyl groups [57]. Figs. 8 indicate the photocatalytic activities of I/TiO_2-T calcined at different temperatures with different I-doping amounts for the degradation of organic pollutants under visible light. Fig. 8a shows the I/TiO_2-T(5/2) catalytic activities calcined at different temperatures. It was observed that the catalyst calcined at 600 °C exhibited the highest catalytic activity for the photodegradation of p-chlorophenol under visible light. Moreover, the I/TiO_2-T with different I-doping amounts for degradation of p-chlorophenol under visible light irradiation was also illustrated in Fig. 8b. The removal rates for the p-chlorophenol pollutant with I/TiO_2-T significantly higher than that of the TiO_2-T and P25-TiO_2. The highest catalytic activity was obtained when iodine was doped on TiO_2-T in the Ti/I molecular ratios of 5/2 and complete removal of p-chlorophenol was achieved at 60 min. However, the removal of the p-chlorophenol with I/TiO_2, TiO_2-T, and P25 catalysts after 140 min reaction were 95.7%, 10.7% and 5.5%, respectively. The photocatalytic degradation of nitrobenzene and phenol were also tested and the results are shown on Fig. 8c–d, respectively. The catalytic activity of I/TiO_2-T(5/2) was much higher

Table 2
The amount of surface acid sites of the catalysts.

Catalyst	TiO_2-T	P-25	I/TiO_2(5/2)	I/TiO_2−T(5/1)	I/TiO_2− T(5/2)	I/TiO_2− T(5/3)
Amount of surface acid-site (mmol/g)	0.063	0.052	0.129	0.105	0.124	0.148

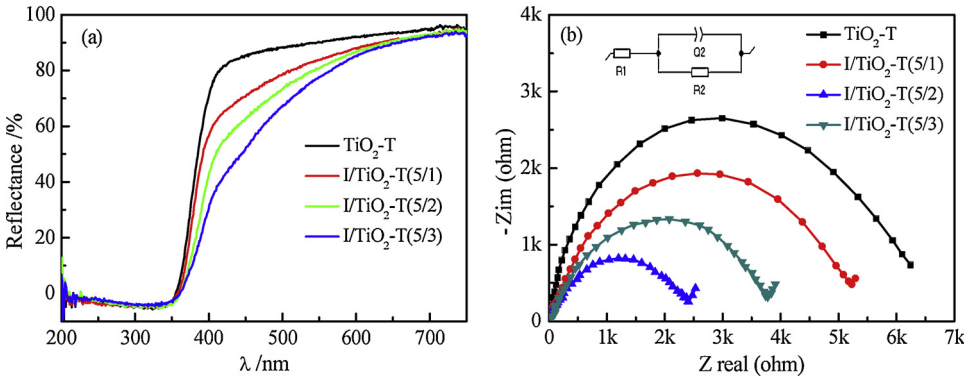

Fig. 5. (a) Diffuse reflectance spectra and (b) Electrochemical impedance spectra and the Randles equivalent circuit for curve fitting (inset) of the TiO_2-T and I/TiO_2-T catalysts with different I-doping amounts.

Table 3
Characteristics of TiO_2 and I/TiO_2-T catalysts.

Sample	Crystalline size /(nm)	S_{BET} /(m^2/g)	Pore volume / (m^3/g)	λ_1 /(nm)	E_{g1} /(eV)	λ_2 /(nm)	E_{g2} /(eV)
TiO_2	30.5	23.0	0.083	386.4	3.21	—	—
TiO_2-T	16.7	121.6	0.296	385.5	3.22	—	—
I/TiO_2(5/2)	17.5	39.7	0.131	390.7	3.17	521.2	2.38
I/TiO_2-T(5/1)	11.1	145.5	0.349	389.6	3.18	495.3	2.50
I/TiO_2-T(5/2)	10.8	149.2	0.350	392.1	3.16	524.7	2.36
I/TiO_2-T(5/3)	10.4	151.8	0.353	395.2	3.14	545.8	2.27

λ_1: 1st adsorption edge; λ_2: 2nd adsorption edge; E_{g1}: 1st energy gap; E_{g2}: 2nd energy gap.

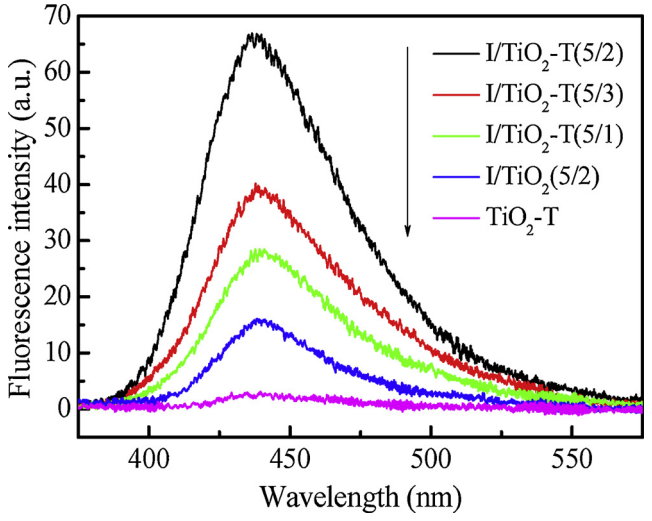

Fig. 6. Fluorescence spectral observed in terephthalic acid solution for TiO_2-T, I/TiO_2, and I/TiO_2-T with different amount of I-doping.

than that of I/TiO_2 and TiO_2-T. The degradation capability of I/TiO_2-T(5/2) order was as follows: p-chlorophenol > phenol > nitrobenzene. The results indicated that the I-doping TiO_2 is the key factor for the visible light catalytic activity and the template-aided fabrication further improves its performance.

The solar light experiments were also performed with plastic wrap which was exposed to the sunlight for testing from 9:00 AM till 3:00 PM in 8 August at Fujian, China and the results are showed in Fig. 9a. It is evident that the I-doping and lignin template significantly increased the sun light photocatalytic activities of TiO_2. In order to determine the reliability in repeated uses, the I/TiO_2-T(5/2) was used repeatedly under photocatalytic runs (Fig. 9b). It can be seen that the catalytic activity of the I/TiO_2-T(5/2) was decreased slightly and 90.7% of the p-chlorophenol degradation was still achieved after 6 runs. Moreover, Fig. 9c also shows the effect of pH on the photocatalytic activity of I/TiO_2-T(5/2) during the p-chlorophenol degradation. It can be observed that the I/TiO_2-T(5/2) displayed an excellent activity under pH value from pH 4 to 8.

In general, the visible light photodegradation of pollutants with I/TiO_2-T can be ascribed by the content of the anatase, the well crystallinity, the formation of defects, and the utilization of lignin template, which makes the catalysts to have higher specific surface area and a smaller grain size [57,65]. The optimum amount of iodine-doping is also important. As we have seen from the catalytic activities (Fig. 8b–d), increasing the I-doping amount did not a guarantee for monotonically increasing the photocatalytic activity. It is also suggested that the DRS analysis results (Fig. 5d) showed the second absorption threshold moving to longer wavelengths and it didn't have the guarantee for the improvement of visible-light photocatalytic activity. Hence, the optimal amount of I-doped in I/TiO_2-T involves the optimal concentration of the photo-induced charge carriers. As it is indicated from the EIS analysis results (Fig. 5b), the electron transfer in the interfaces between electrode and electrolyte were also existed. This electron transfer is due to the photo-induced charge separation. The hydroxyl radical analysis results (Fig. 6) also further confirms the electrons and holes separation. Therefore, the defect concentration needs to be optimized to achieve the best electrical properties and photocatalytic performance.

Moreover, the total organic carbon (TOC) of the pollutants solution were also evaluated at regular intervals of illumination to confirm whether decolourization occurs or the mineralization of the pollutant takes place during the photocatalytic reaction Fig. 10 shows the TOC removal of photocatalytically degraded p-chlorophenol, nitrobenzene, and phenol by P25-TiO_2, TiO_2-T, I/TiO_2 and I/TiO_2-T under visible light at 100 min. As it is indicated from Fig. 10, the amount of the total organic carbon removed was higher in the presence of I/TiO_2-T under visible light. Hence, it is clear from the result that it is not just decolourization but mineralization of the pollutants to occur during photocatalytic reaction.

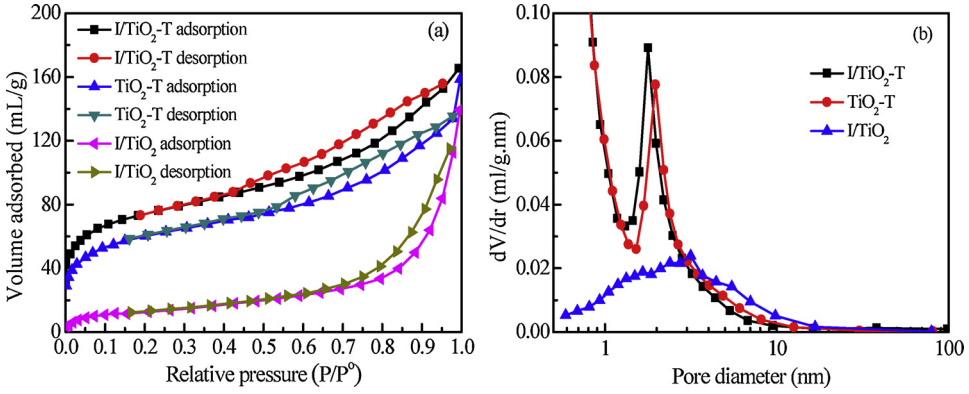

Fig. 7. (a) Nitrogen adsorption-desorption isotherms and (b) pore size distribution curves of the I/TiO_2, TiO_2-T, and I/TiO_2-T.

3.8. Mechanism for cationic I doping enhancement of TiO_2 photocatalytic activity

The incorporation of iodine into TiO_2 involves two kinds of states of cationic I^{5+} in major and anionic I^{1-} in minor, as observed in Fig. 3b. The incorporation of cationic I^{5+} into TiO_2 lattice leads to its substitution for Ti^{4+} lattice with the formation of Ti-O-I bonds and donor defect level in band gap, so the photocatalytic sensitization of TiO_2 responses to the visible light region. The defect symbol in terms of the Kroger-Vink notation is I_{Ti}^{1+} accompanying with one electron, which can be excited to the conduction band for reaction. The incorporation of anionic I^{1-} into TiO_2 leads to its substitution for O^{2-} lattice with the formation of Ti-I-Ti bonds and the donor defect (I_O^{1+} + e^-) in the band gap, so the photocatalytic sensitization of TiO_2 also responses to the visible light region. The DRS analysis in Fig. 5a shows that the higher visible light absorption occurs at the higher I content. However, the higher I content does not guarantee the higher photocatalyst activity, as shown in Fig. 8. An optimum I content is needed to have the best photocatalytic performance. The schematic mechanism for photodegradation of P-chlorophenol, nitrophenol, and phenol is demonstrated in Fig. 11. The reason for an optimum I content in I/TiO_2 involves the optimization in the concentration of the photo–induced charge carriers, i.e. electron and hole, to prolong their lifetime for executing the reactions (1) -˜ (6) to generate OH radical for photodegradation. The I-doping contributes the deep donor level, as supported by the second inflection point at 2.27–2.5 eV in Table 3. The visible light can therefore excite the electrons from the valance band to the donor defect and from the donor defect level to the conduction band. If the I_{Ti}^{1+} concentration is higher than the optimal one obtained with the n(Ti)/n(I) ratio of 5/2, there are more generated electrons

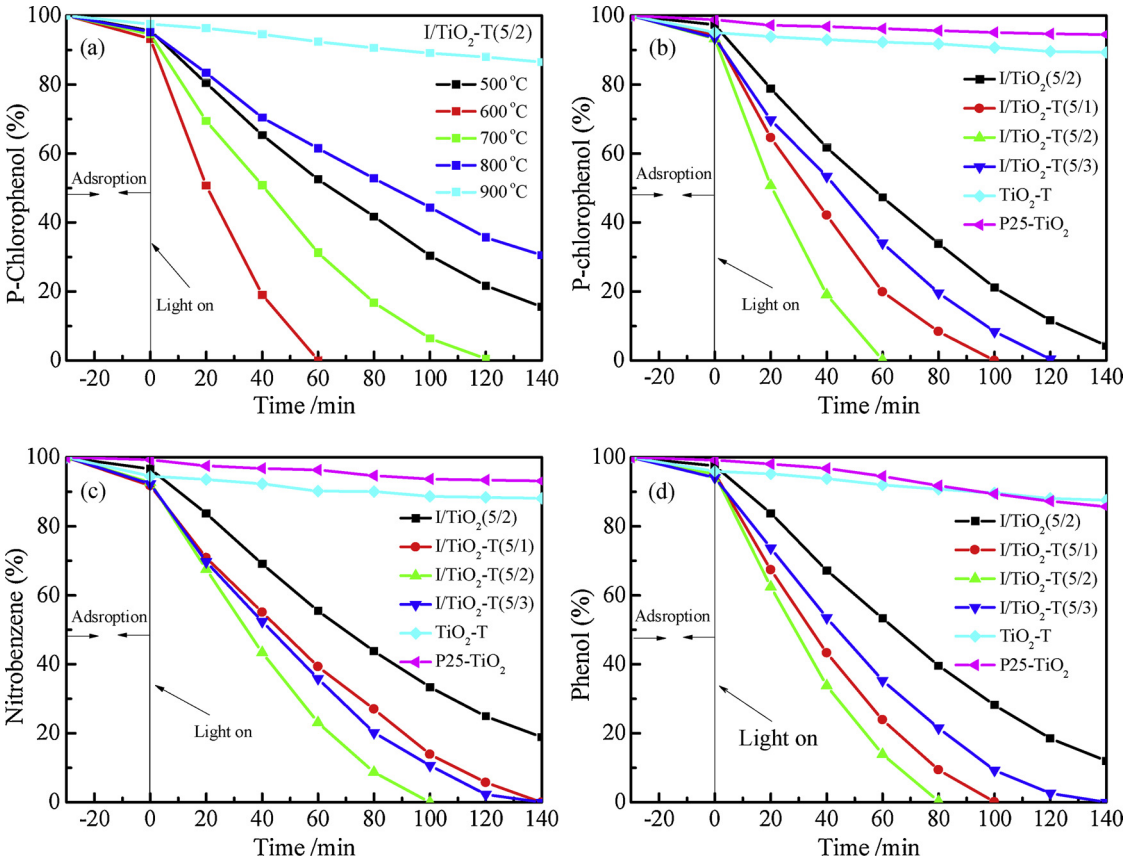

Fig. 8. (a) I/TiO_2-T calcined at different temperatures for the degradation of p-chlorophenol, I/TiO_2-T with different I-doping amounts forthe degradation of (b) p-chlorophenol, (c) nitrobenzene, and (d) phenol under visible light.

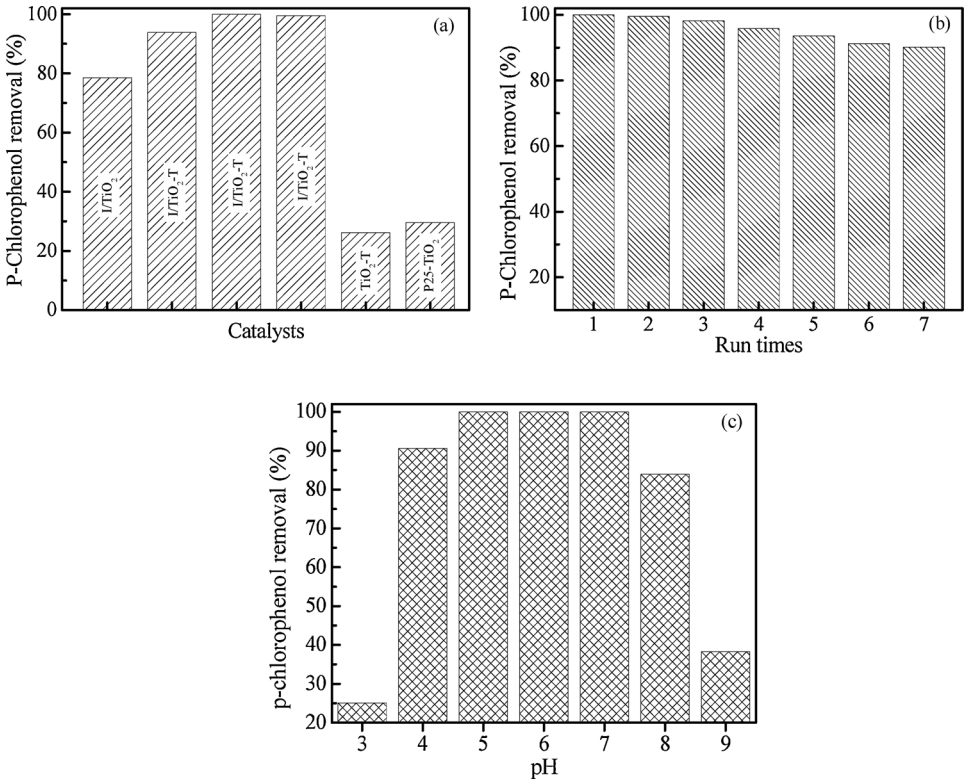

Fig. 9. (a) Photocatalytic activity of I/TiO_2-T with different I doping amounts under solar light. (b) Effect of reusability test on phenol degradation over I/TiO_2-T catalysts. (c) Effect of pH on p-chlorophenol degradation over I/TiO_2-T(5/2).

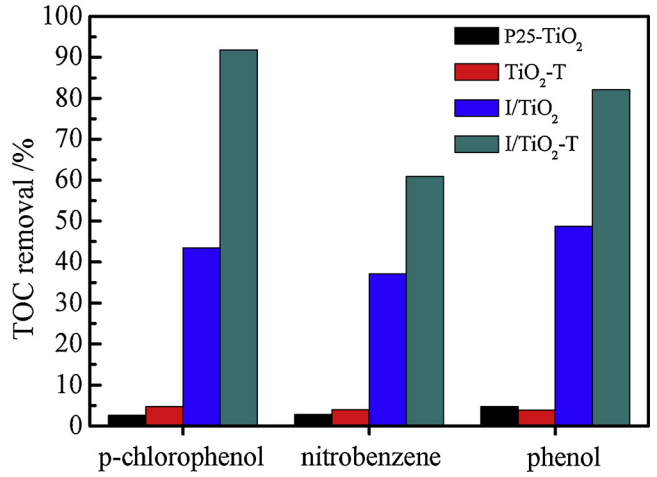

Fig. 10. Total organic carbon (TOC) removal of photocatalytic degradation of p-chlorophenol, nitrobenzene, and phenol by P25-TiO_2, TiO_2-T, I/TiO_2 and I/TiO_2-T under visible light at 100 min.

from the I_{Ti}^{1+} donor level. However, a large amount of excited electrons makes I/TiO_2 much conductive and the fast-transport electrons have more opportunity to recombine with the excited holes and cannot precede the reactions. In the other word, each photo-induced pair has its travel zone. If it has a bigger zone due to the fast transport, the travel zones from different pairs will interact with each other to degrade the lifetime of charge carriers. If the I_{Ti}^{1+} concentration is low, the travel zone is small and the photo-induced carriers are limited to stay in its own zone and can easily collide and recombine together. Therefore, I/TiO_2 with an optimum I content is necessary to achieve the best carrier lifetime and photocatalytic activity. With the available e- and h^+, the active species of OH· radicals can form in Eqs. (1)-(6) for the degradation of toxic species.

3.9. Mechanism for lignin-template synthesis of mesoporous I/TiO_2

The lignin is a three-dimensional network molecule with many hydroxyl functional groups. When the $TiCl_4$ is added into the lignin solution, the strong electron affinity of the positively charged Ti^{4+} metal ions will interact with phenolic hydroxyl group of the lignin. During high temperature annealing process, the growth of TiO_2 is blocked by the three-dimensional network structure of lignin and the hydroxyl group of the lignin. The crystalline growth and grain agglomeration of the TiO_2 precursor will be inhibited [35,38]. It was also reported that the $[Ti(OH)_4]n$ and HIO_3 could be formed in the process of hydrothermal synthesis of I/TiO_2, using titanium source and iodine source. Fig. 12 show the mechanism for the synthesis of I-doped TiO_2 (a) without and (b) with lignin as a template. $TiCl_4$ can be easily hydrolyzed in water to generate the amorphous TiO_2 through the condensation reaction. As the I content in TiO_2 is limited (Table 1), only a few of IO^{3-} species and its decomposed species of I- (Eq. 7) involve the bond formation reactions of Ti-O-I^{5+} and O-Ti-I^{1-} (Fig. 12a). Most of IO^{3-}, I- and IO^{4-} formed in Eq. 7 [42] are not precipitated and are washed away. Due to the 10 nm in size for I/TiO_2, the TiO_2 has the flexibility in incorporation of I^{5+} with a large effective ionic size of 95 pm into the Ti lattice (60.5 pm) in TiO_2, and I^{1-} (220 pm) into the O^{2-} lattice of 140 pm [66]. As the size difference is big, the solubilities of I^{5+} and I^{1-} in TiO_2 are little.

Lignin as a template is rich in hydrogen bond and a hydroxyl macromolecule. When $TiCl_4$ is added dropwise into the uniform dispersion of the lignin suspension, the $TiCl_4$ hydrolyzed product of $Ti(OH)_4$ interacts with lignin to produce bonding on the surface of lignin (Fig. 12b) also interacts with IO^{3-} and I-. TiO_2 precursor in the growth process, affected by the lignin macromolecule is well dispersed and difficult to form the large aggregation. After calcination to remove the lignin template, I/TiO_2 has the much finer crystallite size and a porous structure.

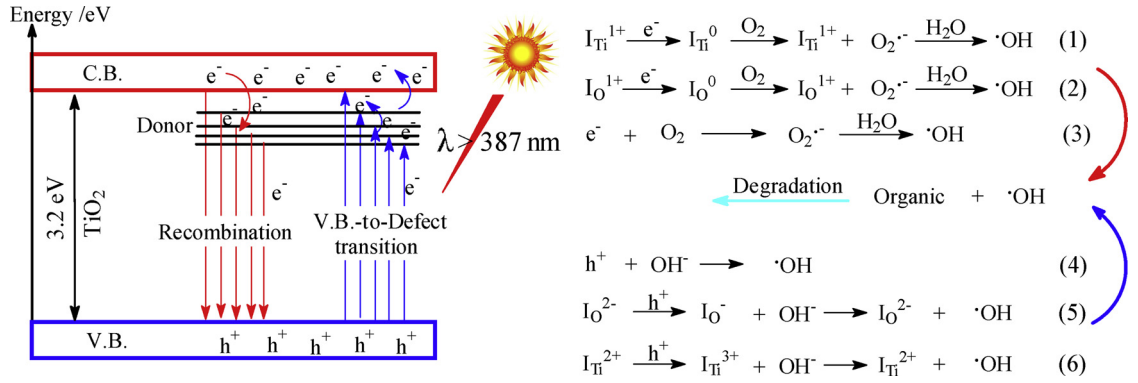

Fig. 11. Schematic mechanism of I-doped TiO_2 for the enhanced photocatalyst activity.

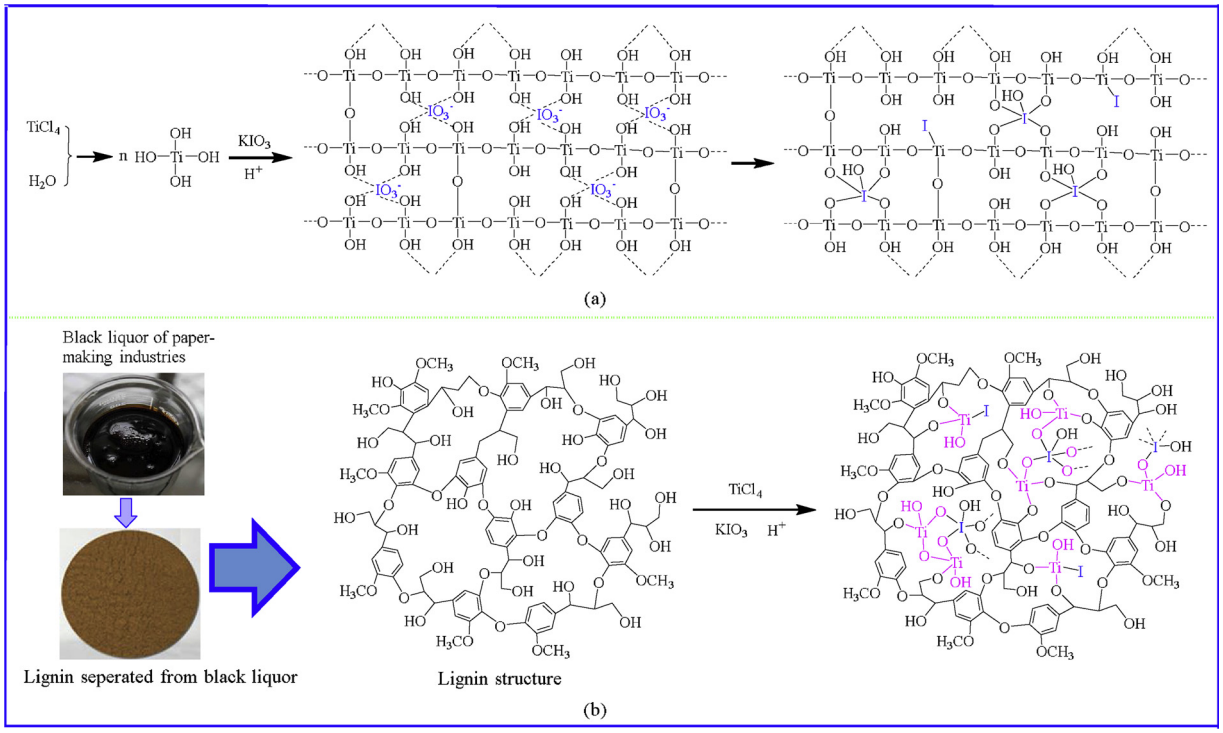

Fig. 12. The proposed mechanism for the synthesis of I-doped TiO_2 (a) without and (b) with lignin as a template.

$$4IO_3^- \rightarrow 3IO_4^- + I^- \quad (7)$$

4. Conclusions

I-doped TiO_2 photocatalyst was synthesized by hydrolysis approach with lignin as a template. The I/TiO_2-T catalyst with an optimum amount of I-doping showed a superior photocatalytic activity under visible and sun light irradiation, as compared to non-template I/TiO_2 or un-doped TiO_2 catalysts. The improvement in the catalytic activity may be attributed by the I-doping that can create Ti-O-I bond with I^{5+} and O-Ti-I bond with I^{1-} in TiO_2, which led to the formation of extrinsic donor defects. Moreover, the utilization of lignin template also changed the morphology and the surface area of the catalysts. The catalytic efficiency of I/TiO_2-T also significantly improved with lignin template and I-doping. Hence, this novel I-doped TiO_2 mesoporous material synthesized in the presence of biological renewable resource of lignin as a template is a promising catalyst in the future.

Acknowledgements

This work was supported by the National Natural Science Foundation of China under the grant No. 31000269, the Strait Postdoctoral Program under the grant No. 1323H0005, and the China Postdoctoral Program under the grant No. 2018M632562.

References

[1] A. Ajmal, I. Majeed, R.N. Malik, M. Iqbal, M.A. Nadeem, I. Hussain, S. Yousaf, G. Zeshan, M.I. Mustafa, M.A. Zafar, Nadeem, Photocatalytic degradation of textile dyes on Cu_2O-CuO/TiO_2 anatase powders, J. Environ. Chem. Eng. 4 (2016) 2138–2146.
[2] W. Peng, X. Wang, X. Li, The synergetic effect of MoS_2 and graphene on Ag_3PO_4 for its ultra-enhanced photocatalytic activity in phenol degradation under visible light, Nanoscale 6 (2014) 8311.
[3] R.J. Tayade, T.S. Natarajan, H.C. Bajaj, Photocatalytic degradation of methylene blue dye using ultraviolet light emitting diodes, Ind. Eng. Chem. Res. 48 (2009) 10262–10267.
[4] P. Bansal, G.R. Chaudhary, S.K. Mehta, Comparative study of catalytic activity of ZrO_2 nanoparticles for sonocatalytic and photocatalytic degradation of cationic and anionic dyes, Chem. Eng. J. 280 (2015) 475–485.
[5] R. Khan, M. Shamshi Hassan, P. Uthirakumar, J.H. Yun, M.S. Khil, I.H. Lee, Facile synthesis of ZnO nanoglobules and its photocatalytic activity in the degradation of

methyl orange dye under UV irradiation, Mater. Lett. 152 (2015) 163–165.
[6] L. Hu, F. Chen, P. Hu, L. Zou, X. Hu, Hydrothermal synthesis of SnO_2/ZnS nanocomposite as a photocatalyst for degradation of Rhodamine B under simulated and natural sunlight, J. Mol. Catal. A-Chem. 411 (2016) 203–213.
[7] X. Li, P. Liu, Y. Mao, M. Xing, J. Zhang, Preparation of homogeneous nitrogen-doped mesoporous TiO_2 spheres with enhanced visible-light photocatalysis, Appl. Catal. B 164 (2015) 352–359.
[8] R. Asahi, T. Morikawa, H. Irie, T. Ohwaki, Nitrogen-doped titanium dioxide as visible-light-sensitive photocatalyst: designs, developments, and prospects, Chem. Rev. 114 (2014) 9824–9852.
[9] Y.C. Zhang, M. Yang, G. Zhang, D.D. Dionysiou, HNO_3-involved one-step low temperature solvothermal synthesis of N-doped TiO_2 nanocrystals for efficient photocatalytic reduction of Cr(VI) in water, Appl. Catal. B 142-143 (2013) 249–258.
[10] Y. Zhang, M. Xu, H. Li, H. Ge, Z. Bian, The enhanced photoreduction of Cr(VI) to Cr (III) using carbon dots coupled TiO_2 mesocrystals, Appl. Catal. B 226 (2018) 213–219.
[11] C.P. Sajan, S. Wageh, A.A. Al-Ghamdi, J. Yu, S. Cao, TiO_2 nanosheets with exposed {001} facets for photocatalytic applications, Nano Res. 9 (2015) 3–27.
[12] J.F. Lei, L.B. Li, X.H. Shen, K. Du, J. Ni, C.J. Liu, W.S. Li, Fabrication of ordered ZnO/TiO_2 heterostructures via a templating technique, Langmuir 29 (2013) 13975–13981.
[13] X. Chen, D.H. Kuo, A.D. Saragih, Z.Y. Wu, H. Abdullah, J. Lin, The effect of the Cu^+/Cu^{2+} ratio on the redox reactions by nanoflower CuNiOS catalysts, Chem. Eng. Sci. 194 (2019) 105–115.
[14] A. Abdelhaleem, W. Chu, Photodegradation of 4-chlorophenoxyacetic acid under visible LED activated N-doped TiO_2 and the mechanism of stepwise rate increment of the reused catalyst, J. Hazard. Mater. 338 (2017) 491–501.
[15] L. Zeng, Z. Lu, M. Li, J. Yang, W. Song, D. Zeng, C. Xie, A modular calcination method to prepare modified N-doped TiO_2 nanoparticle with high photocatalytic activity, Appl. Catal. B 183 (2016) 308–316.
[16] R. Ata, O. Sacco, V. Vaiano, L. Rizzo, G.Y. Tore, D. Sannino, Visible light active N-doped TiO_2 immobilized on polystyrene as efficient system for wastewater treatment, J. Photochem. Photobiol. A-Chem. 348 (2017) 255–262.
[17] Y. Chen, A. Li, Q. Li, X. Hou, L.N. Wang, Z.H. Huang, Facile fabrication of three-dimensional interconnected nanoporous N-TiO_2 for efficient photoelectrochemical water splitting, J. Mater. Sci. Technol. 34 (2018) 955–960.
[18] M. Zalas, Synthesis of N-doped template-free mesoporous titania for visible light photocatalytic applications, Catal. Today 230 (2014) 91–96.
[19] C. Liu, C. Cao, X. Luo, S. Luo, Ag-bridged Ag_2O nanowire network/TiO_2 nanotube array p-n heterojunction as a highly efficient and stable visible light photocatalyst, J. Hazard. Mater. 285 (2015) 319–324.
[20] O.A. Zelekew, D.H. Kuo, J.M. Yassin, K.E. Ahmed, H. Abdullah, Synthesis of efficient silica supported TiO_2/Ag_2O heterostructured catalyst with enhanced photocatalytic performance, Appl. Surf. Sci. 410 (2017) 454–463.
[21] J. He, Q. Liu, Z. Sun, W. Yan, G. Zhang, Z. Qi, P. Xu, Z. Wu, S. Wei, High photocatalytic activity of rutile TiO_2 induced by iodine doping, J. Phys. Chem. C 114 (2010) 6035–6038.
[22] X. Hong, Z. Wang, W. Cai, F. Lu, J. Zhang, Y. Yang, N. Ma, Y. Liu, Visible-light-activated nanoparticle photocatalyst of iodine-doped titanium dioxide, Chem. Mater. 17 (2005) 1548–1552.
[23] S. Khanchandani, S. Kumar, A.K. Ganguli, Comparative study of TiO_2/CuS core/shell and composite nanostructures for efficient visible light photocatalysis, ACS Sustainable Chem. Eng. 4 (2016) 1487–1499.
[24] A. Lisowska-Oleksiak, K. Szybowska, V. Jasulaitiené, Preparation and characterisation of visible light responsive iodine doped TiO_2 electrodes, Electrochim. Acta 55 (2010) 5881–5885.
[25] Q. Zhang, Y. Li, E.A. Ackerman, M. Gajdardziska-Josifovska, H. Li, Visible light responsive iodine-doped TiO_2 for photocatalytic reduction of CO_2 to fuels, Appl. Catal. A Gen. 400 (2011) 195–202.
[26] M. Dorraj, B.T. Goh, N.A. Sairi, P.M. Woi, W.J. Basirun, Improved visible-light photocatalytic activity of TiO_2 co-doped with copper and iodine, Appl. Surf. Sci. 439 (2018) 999–1009.
[27] G. Liu, Z. Chen, C. Dong, Y. Zhao, F. Li, G.Q. Lu, H.M. Cheng, Visible light photocatalyst: iodine-doped mesoporous titania with a bicrystalline framework, J. Phys. Chem. B 110 (2006) 20823–20828.
[28] W. Su, Y. Zhang, Z. Li, L. Wu, X. Wang, J. Li, X. Fu, Multivalency iodine doped TiO_2: preparation, characterization, theoretical studies, and visible-light photocatalysis, Langmuir 24 (2008) 3422–3428.
[29] S. Usseglio, A. Damin, D. Scarano, S. Bordiga, A. Zecchina, C. Lamberti, $(I_2)_n$ Encapsulation inside TiO_2: A way to tune photoactivity in the visible region, J. Am. Chem. Soc. 129 (2007) 2822–2828.
[30] G. Liu, C. Sun, X. Yan, L. Cheng, Z. Chen, X. Wang, L. Wang, S.C. Smith, G.Q. Lu, H.M. Cheng, Iodine doped anatase TiO_2 photocatalyst with ultra-long visible light response: correlation between geometric/electronic structures and mechanisms, J. Mater. Chem. 19 (2009) 2822–2829.
[31] J.C. Colmenares, R.S. Varma, P. Lisowski, Sustainable hybrid photocatalysts: titania immobilized on carbon materials derived from renewable and biodegradable resources, Green Chem. 18 (2016) 5736–5750.
[32] M.A. Mohamed, W.N.W. Salleh, J. Jaafar, Z.A. Mohd Hir, M.S. Rosmi, M. Abd, A.F. Mutalib, M. Ismail, Tanemura, Regenerated cellulose membrane as bio-template for in-situ growth of visible-light driven C-modified mesoporous titania, Carbohydr. Polym. 146 (2016) 166–173.
[33] B.A. Marinho, R.O. Cristóvão, R. Djellabi, J.M. Loureiro, R.A.R. Boaventura, V.J.P. Vilar, Photocatalytic reduction of Cr(VI) over TiO_2-coated cellulose acetate monolithic structures using solar light, Appl. Catal. B 203 (2017) 18–30.
[34] H. Cai, W. Mu, W. Liu, X. Zhang, Y. Deng, Sol–gel synthesis highly porous titanium dioxide microspheres with cellulose nanofibrils-based aerogel templates, Inorg. Chem. Commun. 51 (2015) 71–74.
[35] Y. Zhou, E.-Y. Ding, W.-D. Li, Synthesis of TiO_2 nanocubes induced by cellulose nanocrystal (CNC) at low temperature, Mater. Lett. 61 (2007) 5050–5052.
[36] S. Miao, Z. Miao, Z. Liu, B. Han, H. Zhang, J. Zhang, Synthesis of mesoporous TiO_2 films in ionic liquid dissolving cellulose, Microporous Mesoporous Mater. 95 (2006) 26–30.
[37] X. Chen, D.H. Kuo, D. Lu, N-doped mesoporous TiO_2 nanoparticles synthesized by using biological renewable nanocrystalline cellulose as template for the degradation of pollutants under visible and sun light, Chem. Eng. J. 295 (2016) 192–200.
[38] X. Chen, D.H. Kuo, D. Lu, Y. Hou, Y.R. Kuo, Synthesis and photocatalytic activity of mesoporous TiO_2 nanoparticle using biological renewable resource of un-modified lignin as a template, Microporous Mesoporous Mater. 223 (2016) 145–151.
[39] H.A. Benesi, Acidity of catalyst surfaces. II. Amine titration using hammett indicators, J. Phys. Chem. 61 (1957) 970–973.
[40] T. Hirakawa, Y. Nosaka, Properties of $O_2^{\cdot -}$ and OH· formed in TiO_2 aqueous suspensions by photocatalytic reaction and the influence of H_2O_2 and some ions, Langmuir 18 (2002) 3247–3254.
[41] K. Ishibashi, A. Fujishima, T. Watanabe, K. Hashimoto, Detection of active oxidative species in TiO2 photocatalysis using the fluorescence technique, Electrochem. commun. 2 (2000) 207–210.
[42] W. Wang, Q. Shi, Y. Wang, J. Cao, G. Liu, P. Peng, Preparation and characterization of iodine-doped mesoporous TiO_2 by hydrothermal method, Appl. Surf. Sci. 257 (2011) 3688–3696.
[43] S. Liu, X. Chen, A visible light response TiO_2 photocatalyst realized by cationic S-doping and its application for phenol degradation, J. Hazard. Mater. 152 (2008) 48–55.
[44] D. Li, H. Haneda, N.K. Labhsetwar, S. Hishita, N. Ohashi, Visible-light-driven photocatalysis on fluorine-doped TiO_2 powders by the creation of surface oxygen vacancies, Chem. Phys. Lett. 401 (2005) 579–584.
[45] E.H. Choi, S.I. Hong, D.J. Moon, Preparation of thermally stable mesostructured nano-sized TiO_2 particles by modified sol–gel method using ionic liquid, Catal. Lett. 123 (2008) 84–89.
[46] S.G. Kumar, L.G. Devi, Review on modified TiO_2 photocatalysis under UV/visible light: selected results and related mechanisms on interfacial charge carrier transfer dynamics, J. Phys. Chem. A 115 (2011) 13211–13241.
[47] S. Tojo, T. Tachikawa, M. Fujitsuka, T. Majima, Iodine-doped TiO_2 photocatalysts: correlation between band structure and mechanism, J. Phys. Chem. C 112 (2008) 14948–14954.
[48] M. Long, W. Cai, Z. Wang, G. Liu, Correlation of electronic structures and crystal structures with photocatalytic properties of undoped, N-doped and I-doped TiO_2, Chem. Phys. Lett. 420 (2006) 71–76.
[49] Y. Wang, J. Ren, G. Liu, P. Peng, Synthesis and characterization of iodine ion doped mesoporous TiO_2 by sol–gel method, Mater. Chem. Phys. 130 (2011) 493–499.
[50] M. Pelaez, A.A. de la Cruz, E. Stathatos, P. Falaras, D.D. Dionysiou, Visible light-activated N-F-codoped TiO_2 nanoparticles for the photocatalytic degradation of microcystin-LR in water, Catal. Today 144 (2009) 19–25.
[51] Y. Li, Y. Jiang, S. Peng, F. Jiang, Nitrogen-doped TiO_2 modified with NH_4F for efficient photocatalytic degradation of formaldehyde under blue light-emitting diodes, J. Hazard. Mater. 182 (2010) 90–96.
[52] Q. Ling, J. Sun, Q. Zhou, Preparation and characterization of visible-light-driven titania photocatalyst co-doped with boron and nitrogen, Appl. Surf. Sci. 254 (2008) 3236–3241.
[53] Z. He, L. Xie, J. Tu, S. Song, W. Liu, Z. Liu, J. Fan, Q. Liu, J. Chen, Visible light-induced degradation of phenol over iodine-doped titanium dioxide modified with platinum: role of platinum and the reaction mechanism, J. Phys. Chem. C 114 (2010) 526–532.
[54] Z. He, X. Xu, S. Song, L. Xie, J. Tu, J. Chen, B. Yan, A visible light-driven titanium dioxide photocatalyst codoped with lanthanum and iodine: an application in the degradation of oxalic acid, J. Phys. Chem. C 112 (2008) 16431–16437.
[55] M.R. Hoffmann, S.T. Martin, W. Choi, D.W. Bahnemann, Environmental applications of semiconductor photocatalysis, Chem. Rev. 95 (1995) 69–96.
[56] B. Balasubramanian, K.L. Kraemer, N.A. Reding, R. Skomski, S. Ducharme, D.J. Sellmyer, Synthesis of monodisperse TiO_2 − paraffin core − shell nanoparticles for improved dielectric properties, ACS Nano 4 (2010) 1893–1900.
[57] H. Cui, K. Dwight, S. Soled, A. Wold, Surface acidity and photocatalytic activity of Nb_2O_5/TiO_2 photocatalysts, J. Solid State Chem. 115 (1995) 187–191.
[58] R.P. Barkul, M.K. Patil, S.M. Patil, V.B. Shevale, S.D. Delekar, Sunlight-assisted photocatalytic degradation of textile effluent and Rhodamine B by using iodine doped TiO_2 nanoparticles, J. Photochem. Photobiol. A-Chem. 349 (2017) 138–147.
[59] S. Liu, X. Chen, X. Chen, Preparation of N-doped visible-light response nanosize TiO_2 photocatalyst using the acid-catalyzed hydrolysis method, Chin. J. Catal. 27 (2006) 697–702.
[60] X. Chen, D.H. Kuo, D. Lu, Visible light response and superior dispersed S-doped TiO_2 nanoparticles synthesized via ionic liquid, Adv. Powder Technol. 28 (2017) 1213–1220.
[61] S.X. Liu, X.Y. Chen, X. Chen, A TiO_2/AC composite photocatalyst with high activity and easy separation prepared by a hydrothermal method, J. Hazard. Mater. 143 (2007) 257–263.
[62] X. Zhang, F. Zhang, K.Y. Chan, Synthesis of titania–silica mixed oxide mesoporous materials, characterization and photocatalytic properties, Appl. Catal. A Gen. 284 (2005) 193–198.
[63] K. Ishibashi, A. Fujishima, T. Watanabe, K. Hashimoto, Quantum yields of active oxidative species formed on TiO_2 photocatalyst, J. Photochem. Photobiol. A-Chem. 134 (2000) 139–142.

[64] W. Cai, J. Yu, B. Cheng, B.-L. Su, M. Jaroniec, Synthesis of boehmite hollow core/shell and hollow microspheres via sodium tartrate-mediated phase transformation and their enhanced adsorption performance in water treatment, J. Phys. Chem. C 113 (2009) 14739–14746.
[65] S.K. Pardeshi, A.B. Patil, Effect of morphology and crystallite size on solar photocatalytic activity of zinc oxide synthesized by solution free mechanochemical method, J. Mol. Catal. A-Chem. 308 (2009) 32–40.
[66] R.D. Shannon, Revised effective ionic radii and systematic studies of interatomic distances in halides and chalcogenides, Acta Crystallogr. A 32 (1976) 751–767.